J. Fluid Mech. (2006), *vol.* 565, *pp.* 255–278.
doi:10.1017/S0022112006001819 Printed in the United Kingdom

Stochastic heat transfer enhancement in a grooved channel

By X. WAN AND G. E. KARNIADAKIS†

Division of Applied Mathematics, Brown University, Providence, RI 02912, USA

(Received 20 October 2005 and in revised form 23 March 2006)

We investigate subcritical resonant heat transfer in a heated periodic grooved channel by modulating the flow with an oscillation of random amplitude. This excitation effectively destabilizes the flow at relatively low Reynolds number and establishes strong communication between the grooved flow and the Tollmien–Schlichting channel waves, as revealed by various statistical quantities we analysed. Both single-frequency and multi-frequency responses are considered, and an optimal frequency value is obtained in agreement with previous deterministic studies. In particular, we employ a new approach, the multi-element generalized polynomial chaos (ME-gPC) method, to model the stochastic velocity and temperature fields for uniform and Beta probability density functions (PDFs) of the random amplitude. We present results for the heat transfer enhancement parameter E for which we obtain mean values, lower and upper bounds as well as PDFs. We first study the dependence of the mean value of E on the magnitude of the random amplitude for different Reynolds numbers, and we demonstrate that the deterministic results are embedded in the stochastic simulation results. Of particular interest are the PDFs of E, which are skewed with their peaks increasing towards larger values of E as the Reynolds number increases. We then study the effect of multiple frequencies described by a periodically correlated random process. We find that the mean value of E is increased slightly while the variance decreases substantially in this case, an indication of the robustness of this excitation approach. The stochastic modelling approach offers the possibility of designing 'smart' PDFs of the stochastic input that can result in improved heat transfer enhancement rates.

1. Introduction

Convective heat transfer in grooved channels is a prototype problem, representative of a wide spectrum of engineering applications, such as heat exchangers, biomedical devices, cooling of microelectronic components, etc. It has been found in Ghaddar *et al.* (1986*b*, *c*) that inducing oscillations in the driving flow is an effective approach in improving substantially heat transfer rates. In the past two decades, this method, which is often called resonant heat transfer enhancement, has been widely studied numerically and experimentally (see Ghaddar *et al.* 1986*b*, *c*; Patera & Mikic 1986; Amon & Mikic 1985; Amon *et al.* 1992; Greiner 1991; Herman & Kang 2001; Chung & Tucker 2004, and references therein). In these studies precise sinusoidal excitations were considered and precise knowledge of thermal boundary conditions was assumed. This is particularly important for the numerical simulations, where excitations are

† Author to whom correspondence should be addressed: gk@dam.brown.edu

typically introduced as prescribed deterministic functions. In the current work, we present a new modelling approach for unsteady convective heat transfer, where such constraints are relaxed and the excitations are described as *stochastic processes*. In particular, we study enhancement of heat transfer in a periodic grooved channel due to stochastic excitation. The stochastic simulations allow us to obtain lower and upper bounds of the Nusselt number as well as probability distributions, thus making the comparison of the simulation results with the experimental results more meaningful. In addition, the stochastic analysis readily provides measures of the sensitivity of the system while the richer and high-dimensional stochastic output can aid significantly in gaining deeper understanding of the momentum and heat transport mechanisms.

The simplest approach to stochastic numerical simulations is the Monte Carlo (MC) methods. Due to the slow convergence of MC methods, this approach requires a rather large number of samples, i.e. a large number of solutions of deterministic equations. Perturbation methods have been developed and applied to stochastic mechanics but they are effective only for a small degree of perturbation (see Kaminski & Hien 1999; Kaminski & Carey 2005; Emery 2001).

To model the stochastic velocity and temperature fields, we employ a new method based on *polynomial chaos*, a non-statistical approach to represent stochasticity. Polynomial chaos was pioneered by Wiener (1938) to represent a Gaussian process as the span of Hermite polynomial functionals. Ghanem and Spanos combined Wiener chaos with a finite element method to model uncertainty in solid mechanics (see Ghanem & Spanos 1991; Ghanem 1999*b*, *c*) and also provided the basic framework of the method. A useful extension, termed *generalized polynomial chaos (gPC)*, was proposed in Xiu & Karniadakis (2002) based on the correspondence between the probability density functions (PDFs) of certain random variables and the weight functions of orthogonal polynomials of the Askey scheme. Wiener chaos has also been applied to classical stochastic differential equations (SDEs) with some success, especially on the theoretical front (see Holden *et al.* 1996). For some linear SDEs, such as the diffusion filtering model, Wiener chaos can be effective when integrated with a recursive scheme (see Lototsky, Mikulevicius & Rozovskii 1997). Stochastic Navier–Stokes equations were studied theoretically by Wiener chaos in the recent work of Mikulevicius & Rozovskii (2004). However, in certain applications there are some serious limitations of Wiener chaos and several papers in the literature have focused on this (see Orszag & Bissonnette 1967; Crow & Canavan 1970; Canavan 1970; Kahng & Siegel 1970; Chorin 1974; Hogge & Meecham 1978). Generalized polynomial chaos, including Wiener chaos as a subset, converges to a second-order random process exponentially (p-convergence) with respect to a certain PDF. p-convergence of gPC was studied in Xiu & Karniadakis (2002), Frauenfelder, Schwab & Todor (2005) and Babuška, Tempone & Zouraris (2004).

Along a different line, Deb, Babuška & Oden (2001) employed finite elements in the random space to approximate the stochastic dependence of the solution starting from the deterministic finite element theory. Such an approach shows k-convergence (following the notation in Babuška *et al.* 2004) as the deterministic finite element method does, where k denotes the element size in the random space. In Wan & Karniadakis (2005, 2006), a multi-element generalized polynomial chaos (ME-gPC) approach was proposed, which shows kp-convergence for differential equations with random inputs. That is, ME-gPC combines the polynomial chaos concept with the finite element decomposition approach. Employing adaptivity, ME-gPC can be very effective in dealing with stochastic dynamical systems containing bifurcations, a classical example for which Wiener chaos fails (see Orszag & Bissonnette 1967). One

common property to all the polynomial chaos approaches is that the stochastic differential equation is reduced to a high-dimensional deterministic system by employing a standard Galerkin projection.

In this paper, we employ ME-gPC to study heat transfer enhancement in a two-dimensional grooved channel. This geometry was introduced in Ghaddar *et al.* (1986*b*, *c*) and we use it here for comparisons with corresponding deterministic simulations reported therein. The excitation is an oscillation of *random* amplitude superimposed on the main deterministic flow. Based on the global energy balance presented in Ghaddar, Karniadakis & Patera (1986*a*), we derive proper numerical schemes for the reduced coupled deterministic PDE system from polynomial chaos for fully developed flow. We consider two different stochastic inputs corresponding to uniform and Beta PDFs, and perform simulations at three different Reynolds numbers, i.e. $Re = 225, 525, 825$. We present results for the Nusselt number expressed as a heat transfer enhancement parameter E for different excitation frequencies, where the optimal frequency for heat transfer enhancement is obtained from the mean stochastic response. We study, in particular, the PDFs of E as well as its dependence on the amplitude and the frequency of the excitation. Using some statistics, e.g. variance and correlation, we demonstrate the uncertainty distribution and propagation in the flow field.

This paper is organized as follows. We first provide an overview the ME-gPC approach in the next section. Subsequently, we present the governing Navier–Stokes equations and the corresponding numerical schemes in § 3 including some details, see the two Appendices. In § 4 we present the numerical results and we conclude the paper with a short summary in § 5.

2. Overview of ME-gPC

The polynomial chaos expansion is a spectral representation for second-order random processes using orthogonal polynomials in the random space as the trial basis. The original polynomial chaos proposed by Wiener (1938) employs the Hermite polynomials in the random space as the trial basis. Hermite chaos was employed for solutions of differential equations with stochastic coefficients by Ghanem and Spanos who provided the basic framework. An extension, called 'generalized Polynomial Chaos (gPC)' was introduced in Xiu & Karniadakis (2002, 2003). This extension includes a family of orthogonal polynomials (the so-called Askey scheme) from which the trial basis is selected and can represent non-Gaussian processes more efficiently; it includes the classical Hermite polynomial chaos as a subset. Based on gPC, the multi-element generalized polynomial chaos was developed in Wan & Karniadakis (2005, 2006) to enhance the efficiency of gPC, where the random space is decomposed into random elements and the orthogonal local basis is maintained numerically.

Specifically, a general second-order random process $X(\omega)$ can be expressed by gPC as

$$X(\omega) = \sum_{i=0}^{\infty} \hat{a}_i \Phi_i(\boldsymbol{\xi}(\omega)), \tag{2.1}$$

where ω is the random event and $\Phi_i(\boldsymbol{\xi}(\omega))$ are polynomial functionals of degree p in terms of the d-dimensional random variable $\boldsymbol{\xi} = (\xi_1, \ldots, \xi_d)$. We assume that the ξ_i are independent. The family $\{\Phi_i\}$ is an orthogonal basis with orthogonality relation

$$\mathbb{E}[\Phi_i \Phi_j] = \mathbb{E}[\Phi_i^2]\delta_{ij}, \tag{2.2}$$

where δ_{ij} is the Kronecker delta, and $\mathbb{E}[\cdot]$ denotes the expectation.

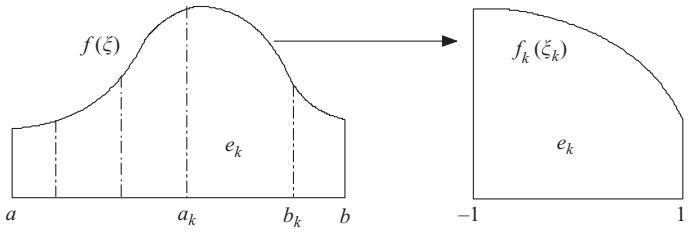

FIGURE 1. Schematic of the decomposition and mapping in the multi-element generalized polynomial chaos (ME-gPC).

For a certain random vector $\boldsymbol{\xi}$, the gPC basis $\{\Phi_i\}$ can be selected in such a way that its weight function has the same form as the PDF of $\boldsymbol{\xi}$. The corresponding type of polynomials $\{\Phi_i\}$ and their associated random variables $\boldsymbol{\xi}$ can be found in Xiu & Karniadakis (2002).

The global gPC expansions work effectively for many physical applications. However, increasing the polynomial order may not be efficient for some problems, e.g. problems with random frequencies or discontinuities. Based on gPC, the multi-element extension (ME-gPC) decomposes the random space into finite elements as in the deterministic finite element methods. The basic idea of ME-gPC is shown in figure 1, where the support $[a, b]$ of the one-dimensional random variable $\boldsymbol{\xi}$ is decomposed into elements $e_k := [a_k, b_k]$. For a d-dimensional case, $e_k := \times_{i=1}^{d} [a_{k,i}, b_{k,i}]$. A new random variable $\boldsymbol{\xi}_k$, $k = 1, 2, \ldots, N$, is defined in each random element, e_k, as

$$\xi_i = \frac{b_{k,i} - a_{k,i}}{2} \xi_{k,i} + \frac{b_{k,i} + a_{k,i}}{2}, \quad i = 1, 2, \ldots, d, \tag{2.3}$$

with a re-scaled PDF (see Wan & Karniadakis 2006)

$$f_k(\boldsymbol{\xi}_k) = \frac{f(\boldsymbol{\xi}(\boldsymbol{\xi}_k))}{Pr(\boldsymbol{\xi} \in e_k)} \prod_{i=1}^{d} \frac{b_{k,i} - a_{k,i}}{2}, \quad k = 1, \ldots, N; i = 1, \ldots, d, \tag{2.4}$$

where N is the number of random elements and $f(\boldsymbol{\xi})$ is the PDF of $\boldsymbol{\xi}$, $Pr(\boldsymbol{\xi} \in e_k) = \int_{e_k} f(\boldsymbol{\xi})\, \mathrm{d}\boldsymbol{\xi}$ is the probability that $\boldsymbol{\xi}$ is located in random element e_k. We note that the support of $\boldsymbol{\xi}_k$ is $[-1, 1]^d$ due to the linear map (2.3). The desired random field $u(\boldsymbol{\xi})$ can be first approximated locally by gPC, where the degree of perturbation is effectively decreased by the linear transform (2.3) from $O(1)$ to $O(\frac{1}{2}(b_{k,i} - a_{k,i}))$. Subsequently, the statistics can be obtained by gathering the information from all random elements

$$\int_B g\,(u(\boldsymbol{\xi}))\, f(\boldsymbol{\xi})\, \mathrm{d}\boldsymbol{\xi} \approx \sum_{k=1}^{N} Pr(\boldsymbol{\xi} \in e_k) \int_{[-1,1]^d} g(\hat{u}_k(\boldsymbol{\xi}_k)) f_k(\boldsymbol{\xi}_k)\, \mathrm{d}\boldsymbol{\xi}_k, \tag{2.5}$$

where B is the support of $\boldsymbol{\xi}$, $g(\cdot)$ is any integrable function of random field $u(\boldsymbol{\xi})$, and $\hat{u}_k(\boldsymbol{\xi}_k)$ is the approximated local random field in element e_k. Formulae for the commonly used statistics are presented in Appendix B.

Since the PDF of $\boldsymbol{\xi}$ is also decomposed together with the random space, the orthogonality of gPC in the entire random space will be, in general, lost in random elements. For uniform random inputs, the Legendre chaos can be employed locally due to the nice properties of uniform distribution; however, for other distributions the local orthogonality can be maintained numerically 'on-the-fly' (see Wan & Karniadakis 2006). For problems related to discontinuity in random space, an adaptive ME-gPC

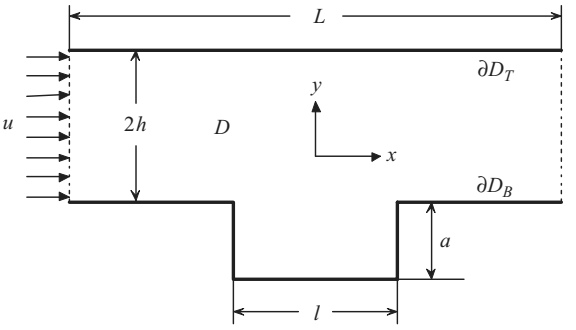

FIGURE 2. Schematic of the geometry of a periodically grooved channel.

scheme first proposed in Wan & Karniadakis (2005) can be adopted to improve the convergence of gPC.

3. Governing equations

The geometry to be considered is shown in figure 2, which is a two-dimensional grooved channel with periodicity length L. The flow is assumed to be fully developed in the x-direction. Natural convection, variation of thermal properties and non-fully developed effects are all assumed to be negligible in this work.

We first define a *stochastic* flow rate condition

$$Q(t;\omega) = \int_{\partial D_B}^{\partial D_T} u(x, y, t;\omega)\,\mathrm{d}y = \tfrac{4}{3}(1 + \eta X(t;\omega)), \tag{3.1}$$

where $X(t;\omega)$ is a second-order random process and η is a constant indicating the degree of perturbation. The value of $Q(t;\omega)$ is independent of x due to mass conservation. We assume that the time average of $X(t;\omega)$ is zero. In particular, we focus on

$$X(t;\omega) = \sum_{i=1}^{M} \xi_i \sin 2\pi\Omega_{F,i}t \tag{3.2}$$

with ξ_i being independent identically distributed (i.i.d.) random variables, in other words, we are considering periodically correlated (*cyclostationary*) random processes (see Gladyshev 1961). In engineering, such random inputs correspond to amplitude modulation of signals. For the flow rate given by (3.1), the time-averaged flow rate is $\bar{Q} = 4/3$, where

$$\bar{Q}(\omega) = \frac{1}{\tau}\int_{t_0}^{t_0+\tau}\left(\int_{x=L} u(y, t;\omega)\cdot\boldsymbol{n}\,\mathrm{d}l\right)\mathrm{d}t. \tag{3.3}$$

with $\boldsymbol{n}$ being the outward normal. We note that by introducing such a random flow rate condition, the velocity field $\boldsymbol{v} = u\hat{\boldsymbol{x}} + v\hat{\boldsymbol{y}}$, the pressure field Π and temperature field T will be random.

For the velocity field we have the incompressible Navier-Stokes equations

$$\frac{\partial \boldsymbol{v}}{\partial t} + (\boldsymbol{v}\cdot\nabla)\boldsymbol{v} = -\nabla\Pi + Re^{-1}\nabla^2\boldsymbol{v} \quad \text{in } D, \tag{3.4a}$$

$$\nabla\cdot\boldsymbol{v} = 0 \quad \text{in } D, \tag{3.4b}$$

where $Re = 3\bar{Q}/4\nu$ is the Reynolds number with ν being the kinematic viscosity. The appropriate boundary conditions for the velocity are

$$\boldsymbol{v}(x,t;\omega) = 0 \quad \text{on } \partial D_T \text{ and } \partial D_B, \tag{3.5a}$$

$$\boldsymbol{v}(x,y,t;\omega) = \boldsymbol{v}(x+L,y,t;\omega), \tag{3.5b}$$

corresponding to no-slip and periodicity, respectively. For the pressure we require that (see Ghaddar *et al.* 1986*a*)

$$\Pi(\boldsymbol{x},t;\omega) = -\Pi^x(t;\omega)x + \hat{\Pi}(\boldsymbol{x},t;\omega), \tag{3.6a}$$

$$\hat{\Pi}(x,y,t;\omega) = \hat{\Pi}(x+L,y,t;\omega). \tag{3.6b}$$

For the temperature field $T(\boldsymbol{x},t;\omega)$ the convection equation can be expressed in conservation form as

$$\frac{\partial T}{\partial t} + \nabla\cdot(\boldsymbol{v}T) = (Re\,Pr)^{-1}\nabla^2 T, \tag{3.7}$$

where $Pr = \nu/\alpha$ is the Prandtl number with α being the thermal diffusivity. We first subtract a linear term from T, which yields

$$T(\boldsymbol{x},t;\omega) = \gamma(\omega)x + \theta(\boldsymbol{x},t;\omega). \tag{3.8}$$

We extend the global conservation of energy presented in Ghaddar *et al.* (1986*a*) to a stochastic case and obtain the unknown term $\gamma(\omega)$ as

$$\gamma(\omega) = \frac{\alpha q'(\omega)}{\kappa\,\bar{Q}(\omega)L}, \tag{3.9}$$

where κ is the thermal conductivity of the fluid and q' is the total heat transfer rate into the domain

$$q'(\omega) = \int_{\partial D} q''(\boldsymbol{x};\omega)\,\mathrm{d}l. \tag{3.10}$$

Here $q''(\boldsymbol{x};\omega)$ denotes the heat flux at the boundaries. In terms of θ, equation (3.7) can be written as

$$\frac{\partial\theta}{\partial t} + \nabla\cdot(\boldsymbol{v}(\theta+\gamma x)) = (Re\,Pr)^{-1}\nabla^2\theta \tag{3.11}$$

subject to the following boundary conditions:

$$\kappa\nabla\theta\cdot\boldsymbol{n} = q''(\boldsymbol{x}) - \kappa\gamma n_x \quad \text{on } \partial D_T \text{ and } \partial D_B, \tag{3.12a}$$

$$\theta(x,y,t;\omega) = \theta(x+L,y,t;\omega), \tag{3.12b}$$

where n_x is the component of $\boldsymbol{n}$ in the x-direction.

The random fields $\boldsymbol{v}(\boldsymbol{x},t;\omega)$, $\Pi(\boldsymbol{x},t;\omega)$ and $\theta(\boldsymbol{x},t;\omega)$ are modelled by ME-gPC in this work. In Appendix A, we present the ME-gPC expansions of the governing equations. The physical space is discretized by a spectral/hp element method (see Karniadakis & Sherwin 2005) and a typical mesh is shown in figure 3, where 42 elements and eighth-order Jacobi polynomials are used to obtain converged results.

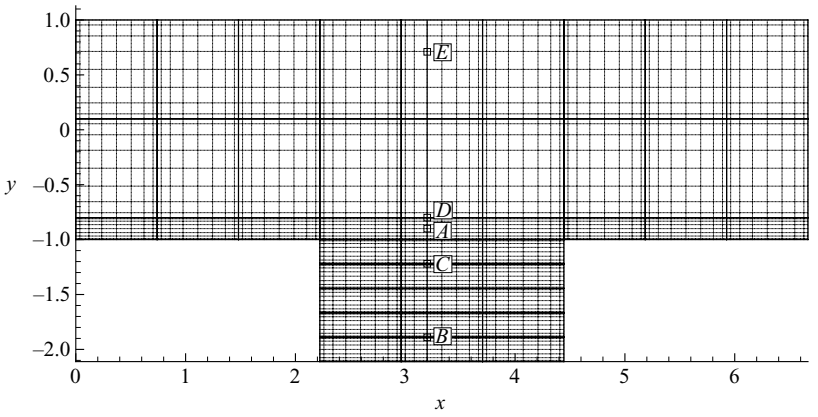

FIGURE 3. A typical spectral/*hp* element mesh for the physical discretization. The dotted lines are based on quadrature points of Jacobi polynomials. The reference points *A*–*E* defined along the straight line $x = 3.2$ are used in § 4.5.

Re	*Pr*	*L*	*l*	*a*
225–825	1.0	6.6666	2.2222	1.1111

TABLE 1. Physical parameters used in this work. The lengths are non-dimensionalized with the channel half-width *h*.

4. Numerical results

4.1. *Notation*

To get an overall measure of the transport characteristics of the fully developed flow, we first define a time-averaged global Nusselt number *Nu* as in Ghaddar *et al.* (1986*c*)

$$Nu(\omega) = L\left(1 + \frac{2a}{L}\right)^2 \Big/ \int_{\partial D_B} \langle \theta(\omega) - \theta_b(\omega) \rangle_t \, \mathrm{d}s|_{\partial D_B}, \tag{4.1}$$

where θ_b is a reference temperature taken to be the (periodic part of the) mixed-mean temperature at $x = 0$,

$$\theta_b(\omega) = \left\langle \frac{\int_{\partial D_B}^{\partial D_T} u(x = 0, y, t; \omega)\theta(x = 0, y, t; \omega) \, \mathrm{d}y}{Q(t; \omega)} \right\rangle_t, \tag{4.2}$$

and $\langle \rangle_t$ refers to the time-average over a cycle of the flow, $t < t' < t + \Omega_F^{-1}$. The transport enhancement parameter is defined as

$$E = \frac{Nu(Re, \eta, Pr)}{Nu(Re, \eta = 0, Pr)}. \tag{4.3}$$

For the purpose of comparison, the parameters in table 1 are the same as those in Ghaddar *et al.* (1986*c*).

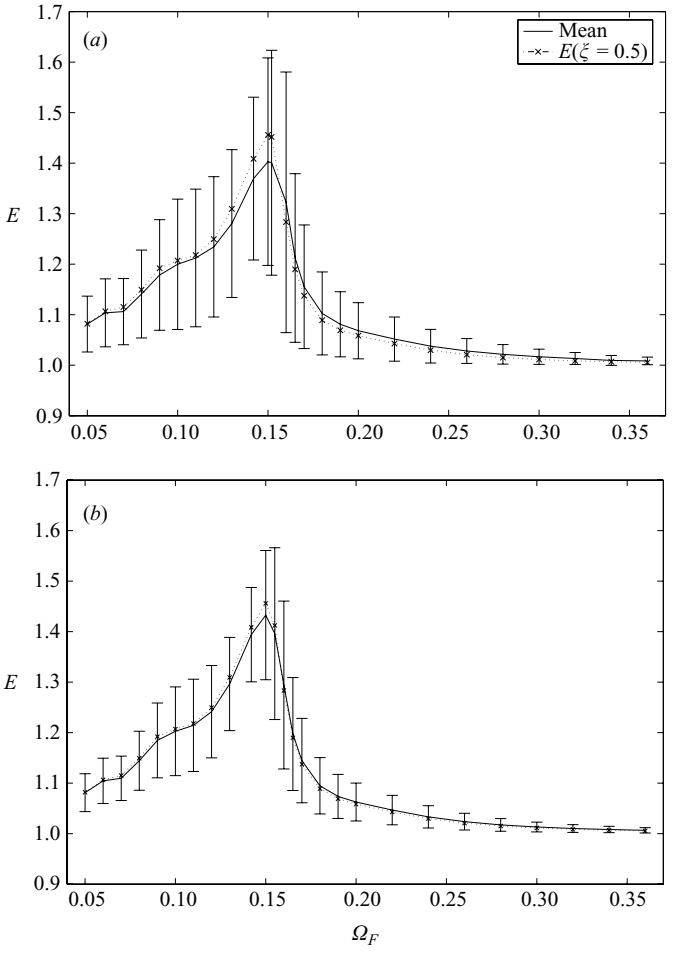

FIGURE 4. Mean of E with error bars indicating the standard deviation for uniform (a) and Beta (b) random inputs. $E(\bar{\xi} = 0.5)$ is the deterministic solution for the mean input. $Re = 525$.

4.2. *Mean values and bounds of E*

We first assume that in the random flow rate condition (3.1) $X(t;\omega)$ takes the simple form

$$X(t;\omega) = \eta\xi \sin 2\pi\Omega_F t, \tag{4.4}$$

where ξ is a random variable defined in $[0, 1]$ and $\eta = 0.2$. Compared to $\bar{Q}$, the mean amplitude $\eta\bar{\xi} = 0.1$ indicates 10% perturbation. For the random amplitude the coefficient of variance is $\sigma_a/\mathbb{E}[\eta\xi] = 58\%$ for the uniform distribution and 38% for the $Beta(2, 2)$ distribution, where σ_a is the standard deviation of $\eta\xi$.

In figure 4, we show the mean of E with 'error bars' for *uniform* (upper) and *Beta* (lower) random inputs at different excitation frequencies, where both the upper and lower error ranges are equal to the standard deviation of E. ME-gPC up to $N = 3$ and $p = 5$ is employed to ensure the numerical convergence. We first examine the results for the uniform random inputs. We observe that the mean of E is sensitive to the frequency of excitation force, and the maximum value is reached at $\Omega_F \approx 0.15$. For comparison, we also show the corresponding deterministic solutions

at $E(\bar{\xi} = 0.5)$, where 0.5 is the mean of the uniform random variable ξ. We can see that the mean of E for different frequencies does not coincide with the corresponding deterministic solution, since the relation between ξ and E is nonlinear. Furthermore, $E(\bar{\xi} = 0.5) \geqslant \bar{E}$ when $\Omega_F \leqslant 0.16$; otherwise, $E(\bar{\xi} = 0.5) \leqslant \bar{E}$. This means that the relation between E and ξ changes for different frequencies. However, the deterministic and stochastic mean solutions give the same optimal frequency. As Ω_F approaches 0.15, the standard deviation increases gradually. This can be interpreted as a result of sensitivity of the heat transfer enhancement to the excitation frequency. Also, it is seen that the difference between $\bar{E}$ and $E(\bar{\xi} = 0.5)$ reaches a maximum value at $\Omega_F = 0.15$. For Beta random inputs, similar properties are observed.

In Ghaddar *et al.* (1986*b*), it was found that the least-stable modes of grooved channel flow closely resemble Tollmien–Schlichting channel waves. The frequency Ω_1 of the first least-stable mode can be predicted by the Orr–Sommerfeld dispersion relation; it is 0.142 for the geometry used in this work. In Ghaddar *et al.* (1986*c*), it was verified that the optimal frequency for heat transfer enhancement is consistent with the Tollmien–Schlichting frequency for the linear system and shifts a little for the nonlinear system. The optimal frequency $\Omega_F = 0.15$ given by the polynomial chaos method agrees well with the aforementioned deterministic studies. We note that the standard deviation (indicated by the length of 'error bars') of E does not reach the maximum value at $\Omega_F = 0.15$ as the mean does. The excitation frequency for the largest standard deviation is actually a little larger than $\Omega_F = 0.15$. This implies that the optimal frequency depends on the amplitude. Since the mean of E has a maximum value at $\Omega_F = 0.15$, we know that

$$\frac{\partial \bar{E}}{\partial \Omega_F}\bigg|_{\Omega_F=0.15} = \int_0^1 \frac{\partial E}{\partial \Omega_F} f(\xi)\,\mathrm{d}\xi|_{\Omega_F=0.15} = 0, \tag{4.5}$$

where $f(\xi)$ is the PDF of ξ. We now consider the first-order derivative of the variance of E in terms of Ω_F:

$$\frac{\partial\left(\sigma_E^2\right)}{\partial \Omega_F} = 2\int_0^1 E\frac{\partial E}{\partial \Omega_F} f(\xi)\,\mathrm{d}\xi - 2\left(\int_0^1 E f(\xi)\,\mathrm{d}\xi\right)\left(\int_0^1 \frac{\partial E}{\partial \Omega_F} f(\xi)\,\mathrm{d}\xi\right). \tag{4.6}$$

Assuming that the optimal frequency does not depend on the amplitude, say, for any ξ the optimal frequency is $\Omega_F = \Omega_M$, we then have for any ξ

$$\frac{\partial E}{\partial \Omega_F}\bigg|_{\Omega_F=\Omega_M} = 0, \tag{4.7}$$

which implies that both the mean and standard deviation of E should reach the maximum values at $\Omega_F = \Omega_M$. However, this contradicts the numerical results in figure 4. Thus, the optimal frequency should vary in terms of the amplitude. In figure 5, we demonstrate the dependence of optimal frequency on the amplitude using deterministic simulations, where it can be seen that the optimal frequency for amplitude 0.1 is 0.15 whereas it is 0.163 for amplitude 0.2. In Ghaddar *et al.* (1986*c*) the excitation force with an amplitude 0.2 was studied and an optimal frequency for the nonlinear system was found to be 0.168, which agrees very well with our result 0.163.

The above observations show that the choice of exact optimal frequency is a complicated problem, which is related to many factors. When randomness is present, a better way to select the optimal frequency is to check the mean response since it is more reasonable to assume that a factor, e.g. the amplitude, is random with a certain PDF.

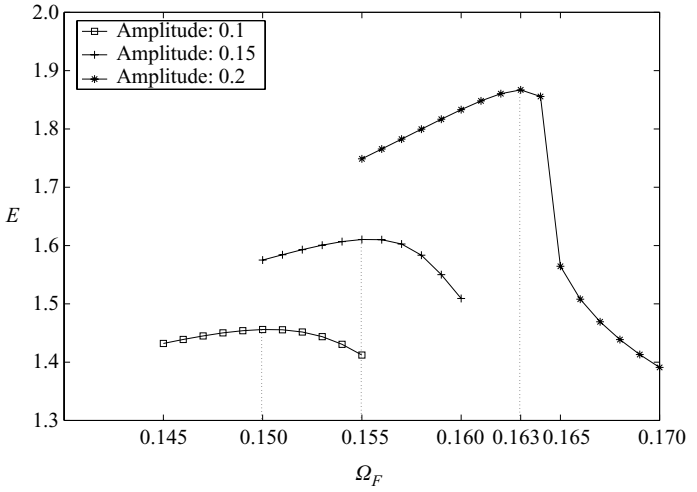

FIGURE 5. Dependence of the optimal frequency on the amplitude at $Re = 525$.

4.3. *Probability density functions of E*

We now study the PDFs of the transport enhancement parameter E under different types of random inputs. We study here only the case with $\Omega_F = 0.15$, which corresponds to the maximum response for $\eta = 0.2$. Based on the solutions of polynomial chaos, all PDFs shown in this section are obtained by a standard Monte Carlo method with 1 000 000 realizations.

First, we assume that ξ is a uniform random variable, i.e. $\xi \sim U[0, 1]$, and let $E = E(\xi)$. Using the properties of the PDF, we obtain the PDF of E

$$f_E(E) = E^{(1)}(\xi(E))^{-1}, \tag{4.8}$$

where superscript (n) indicates the nth-order derivative. The first-order derivative of f_E can be obtained from the chain rule of calculus as

$$f_E^{(1)}(E) = -\frac{E^{(2)}(\xi(E))}{E^{(1)}(\xi(E))^3}. \tag{4.9}$$

We now examine the PDF of E at $Re = 225$, which is shown in figure 6. The PDF of E is not uniform, unlike the input, and has a minimum at $E \approx 1.15$, which means that the second-order derivative of $E(\xi)$ should be zero at $E \approx 1.15$ according to equation (4.9). Thus, the support of E can be roughly divided into two parts:

Part I: $1 \leqslant E \leqslant 1.15$, where the probability density decreases and the first-order derivative of f_E increases to zero.

Part II: $E \geqslant 1.15$, where the probability density increases and the first-order derivative of f_E increases from zero.

Similar phenomena were shown in Ghaddar *et al.* (1986*c*) for deterministic simulations at $Re = 225$. We next check the local behaviour of E. For $\xi \ll 1$ (E is around 1), we assume that

$$E - 1 \sim c\xi^{\beta}, \quad c \text{ is constant.} \tag{4.10}$$

It is easy to obtain the PDF of E as

$$f_E(E) \sim c_E(E-1)^{(1-\beta)/\beta}, \tag{4.11}$$

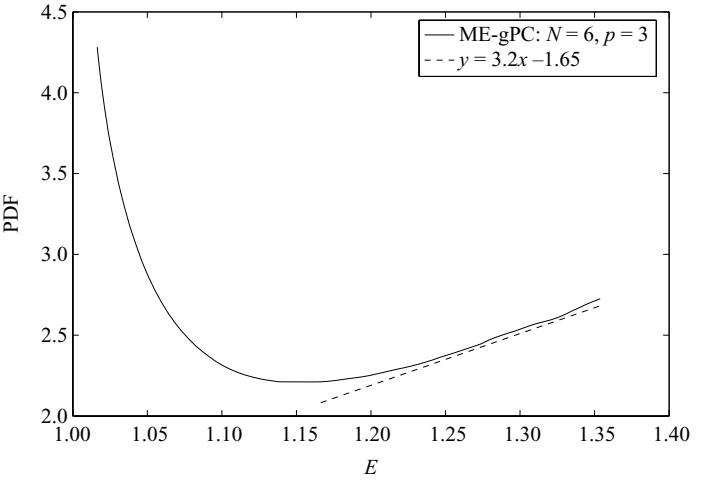

FIGURE 6. PDF of E with uniform random inputs. $Re = 225$.

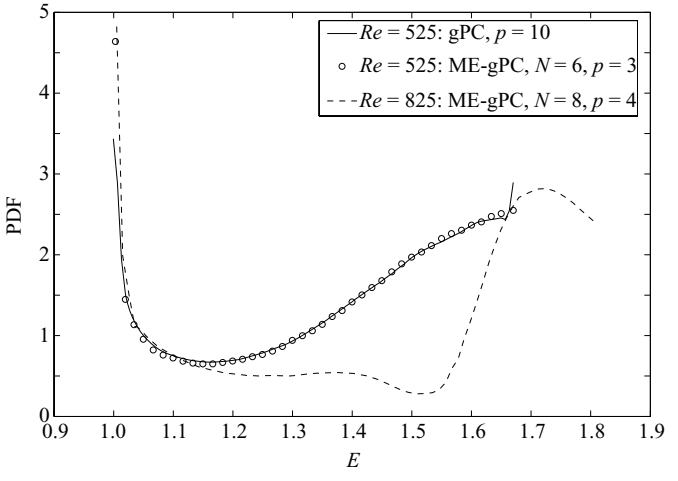

FIGURE 7. PDF of E with uniform random inputs at $Re = 525, 825$.

where c_E is constant. Due to the singularity at $E = 1$, we obtain that $\beta > 1$ consistent with the deterministic estimation in Ghaddar *et al.* (1986*c*), where β is set to be 2 for small amplitudes. As the amplitude increases, such an estimate will be not valid. We know that $E^{(2)}(\xi) = 0$ when $E \approx 1.15$. However, the second-order derivative of $E(\xi) = c\xi^2$ is a non-zero constant, which is a contraction. Similarly, we analyse the part corresponding to large amplitudes with the assumption $E \sim c_1\xi^\beta + c_2$, which yields

$$f_E(E) \sim c_E(E - c_2)^{(1-\beta)/\beta}. \tag{4.12}$$

From figure 6, we can see that $(1 - \beta)/\beta \approx 1$ for large E, which yields $\beta = \frac{1}{2}$. Such a result is the same as the deterministic estimation in Ghaddar *et al.* (1986*c*).

In figure 7, we show the PDFs of E at $Re = 525$ and 825. For comparison we include the results from high-order gPC. We use ME-gPC with a six-element mesh [0, 0.1, 0.3, 0.5, 0.7, 0.9, 1] (in random space) for $Re = 525$ and an eight-element mesh [0, 0.1, 0.3, 1.1/3, 1.3/3, 0.5, 0.7, 0.9, 1.0] for $Re = 825$. A similar two-part structure

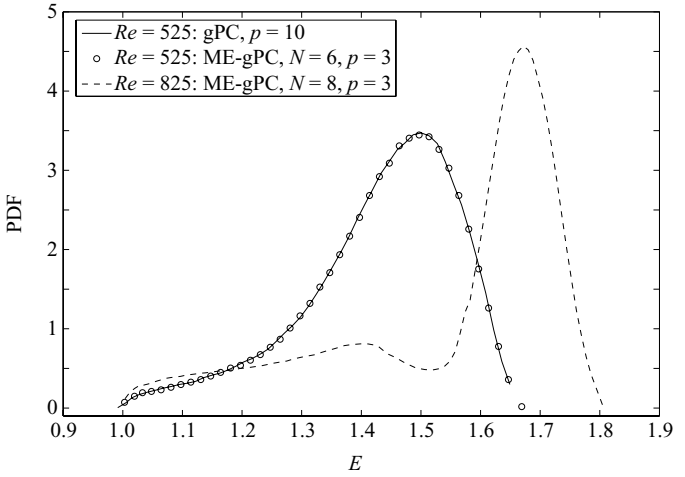

FIGURE 8. PDF of E with Beta random inputs at $Re = 525, 825$.

Re	s_E(Uniform)	k_E(Uniform)	s_E(Beta)	k_E(Beta)
225	0.10	1.65	0.05	2.13
525	−0.61	2.14	−0.88	3.51
825	−0.68	1.87	−1.20	3.30

TABLE 2. Skewness s_E and kurtosis k_E of E for different random inputs and Reynolds numbers.

is observed in the PDF for $Re = 525$ but differences arise in the PDF for $Re = 825$. For large E, the relation between E and probability density is not linear any more and becomes more complicated as the Reynolds number increases. For example, in the range $E \geqslant 1.4$, $f_E^{(1)}(E) > 0$ for $Re = 525$ while $f_E^{(1)}(E) = 0$ at $E = 1.52$ and 1.72 for $Re = 825$. Using equation (4.9), we know that there exist two stationary points in the curve $E = E(\xi)$ for $Re = 825$ but no stationary points for $Re = 525$.

As a representative non-uniform random input, we consider the Beta distribution $Beta(2, 2)$ in $[0, 1]$. In figure 8, the PDFs of E are shown for $Re = 525$ and 825. We use the same meshes as before for ME-gPC. Compared to the symmetric PDF of $Beta(2, 2)$, the PDFs of E have a clear bias towards larger E and the bias shifts further as the Reynolds number increases. In table 2 we present the skewness s_E and kurtosis k_E of E for different random inputs and Reynolds numbers. In particular, we notice the negative s_E for $Re = 525, 825$ with the absolute values increasing with Re. In other words, an asymmetric tail extending out to the left becomes stronger with Re.

Although the PDF of E is not symmetric, unlike the PDF of random inputs, it appears that we can estimate the mean of E using $E(\bar{\xi} = 0.5)$ for a moderate perturbation ($\eta = 0.2$), where $\bar{\xi} = 0.5$ is the mean of ξ. In table 3, we compare the mean of E and deterministic results $E(\bar{\xi} = 0.5)$, where the percentage of difference is also given. We can see that the difference is less than 10% for both uniform and Beta random inputs in the range $Re \in [225, 825]$. For certain random inputs, the difference increases with the Reynolds number; for a fixed Reynolds number, the difference for the uniform inputs is larger than that for the Beta inputs because the

Re	$\bar{E}$(Uniform)	σ_E(Uniform)	$\bar{E}$(Beta)	σ_E(Beta)	$E(0.5)$
225	1.1694(0.28%)	0.1196	1.1664(0.00%)	0.0829	1.1661
525	1.4045(3.65%)	0.2058	1.4344(1.60%)	0.1281	1.4577
825	1.5014(8.41%)	0.2766	1.5945(2.73%)	0.1945	1.6393

TABLE 3. The mean and standard deviation of E for different random inputs and the corresponding deterministic E with the mean random inputs.

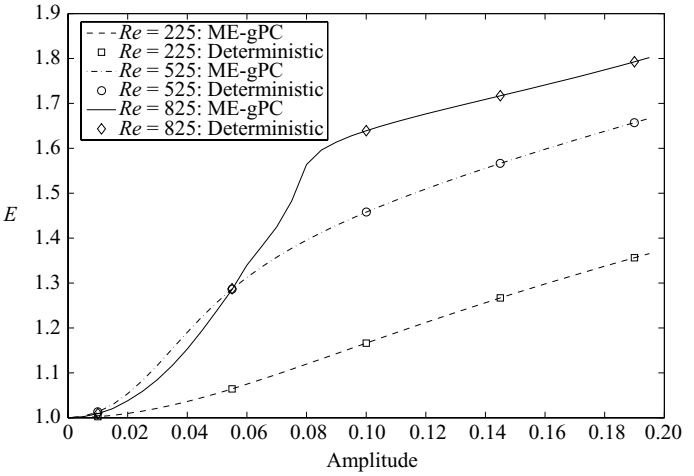

FIGURE 9. Curves of the enhancement ratio E versus the excitation amplitude for different Reynolds numbers.

PDF of $Beta(2, 2)$ distribution has a maximum at $\xi = 0.5$ and decreases to zero at the ends. However, such an approximate analysis is not expected to be valid for general random inputs with non-symmetric PDFs.

Since the stochastic amplitude is a random variable, any individual realization of the ME-gPC should correspond to a deterministic simulation; in figure 9 we plot the E-amplitude curves based on the ME-gPC solutions for different Reynolds number, where we also compare the ME-gPC predictions with deterministic simulations at some reference points. We see that the deterministic solutions are indeed included in the stochastic solutions. In deterministic simulations the common approach to study the E-amplitude relation is to interpolate the results of E at different amplitudes. However, such a procedure will usually involve many individual deterministic simulations to get a good approximation. Thus, ME-gPC provides an effective approach not only for stochastic studies but also for obtaining deterministic relations economically.

4.4. *Effect of different frequencies on E*

Given a periodic covariance kernel $K(t, s) = K(t + T, s + T)$, a second-order periodically correlated random process can be expressed by the Karhunen–Loeve (K-L) decomposition, which takes a form

$$X(t) = \sqrt{\frac{\lambda_0}{T}}\xi_{0,0} + \sqrt{\frac{2}{T}}\sum_{n=1}^{\infty}\sqrt{\lambda_n}\left[\xi_{n,1}\cos\frac{2n\pi}{T}t + \xi_{n,2}\sin\frac{2n\pi}{T}t\right], \tag{4.13}$$

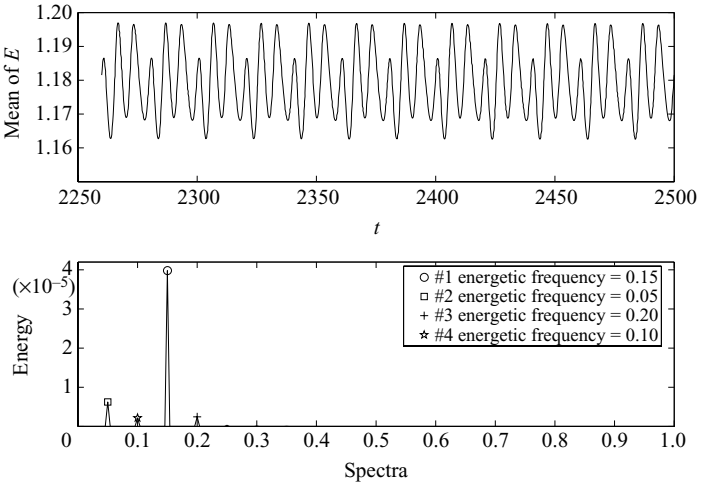

FIGURE 10. Spectra of the mean of E at $Re = 525$ for case (I). $\Omega_{F_i} = 0.1, 0.15, 0.2$.

where T is the period and $\{\xi_{i,j}\}$ is a set of uncorrelated random variables. The eigenvalues $\{\lambda_i\}$ can be determined by the correlation length and Fourier coefficients of the kernel $K(t, s)$ (see Lucor 2004). We assume that the first eigenvalue $\lambda_0 = 0$ since the corresponding eigenfunction is constant.

To focus on the interaction between $\Omega_F = 0.15$ and other frequencies, we first assume that the energy of each mode is of the same order and consider the following random condition:

$$Q(t) = \frac{4}{3}\left(1 + \frac{0.2}{3}\sum_{i=1}^{3} a_i \xi_i \sin(2\pi\Omega_{F,i} t)\right), \tag{4.14}$$

where $\xi_i \sim U[0, 1]$ are uniform i.i.d. random variables and $a_i = 0$ or 1. In other words, we impose three frequencies with i.i.d. random amplitudes in the excitation force. The Reynolds number is set to $Re = 525$.

We investigate in detail two cases:

$$\text{(I): } \Omega_{F,i} = 0.10, 0.15, 0.20 \text{ and (II): } \Omega_{F,i} = 0.11, 0.15, 0.18.$$

For both cases, we set $a_i = 1, i = 1, 2, 3$, which means that the standard deviation of each random amplitude is the same. We use ME-gPC with $N = 3 \times 4 \times 3 = 36$ and $p = 2$ to resolve the problem, where uniform meshes in each random dimension are employed. We select frequencies according to figure 4: frequencies that introduce smaller heat transfer enhancement are chosen as a perturbation of the frequency $\Omega_F = 0.15$.

We plot the spectra of mean and standard deviation of E in figures 10 and 11 for case (I), and in figures 12 and 13 for case II, based on the ME-gPC solutions. We note that

(i) frequency $\Omega_F = 0.15$ is dominant;

(ii) a linear combination of other frequencies with $\Omega_F = 0.15$ is present.

It appears that there exists a non-trivial interaction between $\Omega_F = 0.15$ and other frequencies. For case (I), a subharmonic frequency 0.05 emerges in the spectra of mean and standard deviation; for case (II), more frequencies, e.g. 0.03 and 0.04, are

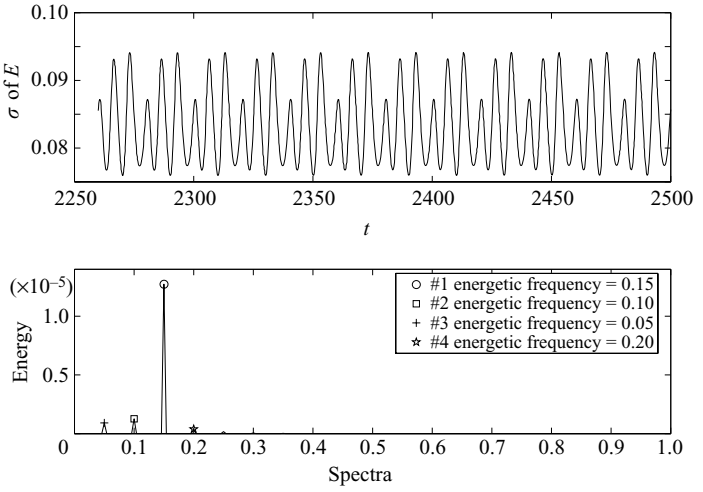

FIGURE 11. Spectra of the standard deviation of E at $Re = 525$ for case (I). $\Omega_{F_i} = 0.1, 0.15, 0.2$.

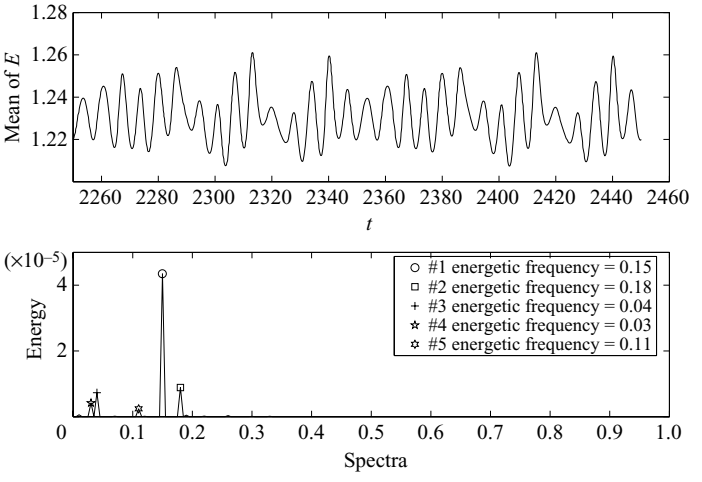

FIGURE 12. Spectra of the mean of E at $Re = 525$ for case (II). $\Omega_{F_i} = 0.11, 0.15, 0.18$.

involved. Since the energy from frequencies other than $\Omega_F = 0.15$ is small, the heat transfer enhancement will be determined mostly by the frequency $\Omega_F = 0.15$.

In tables 4 and 5, we compare the mean and standard deviation of E for different random inputs. Since $\Omega_F = 0.15$ is the dominant frequency, we focus on the difference between one-dimensional random inputs with $\Omega_F = 0.15$ (corresponding to $(a_1, a_2, a_3) = (0, 1, 0)$) and the aforementioned two cases. The difference in mean is 2.7% and 3.4%, respectively, and the difference in standard deviation is 27% and 28%, respectively. In other words, the mean of E is almost unchanged while the standard deviation is effectively reduced. Thus, it appears that the imposed frequencies, other than $\Omega_F = 0.15$, have a much stronger influence on the standard deviation of E than on the mean value. Such a phenomenon should be the consequence of the previously mentioned interaction between $\Omega_F = 0.15$ and other frequencies.

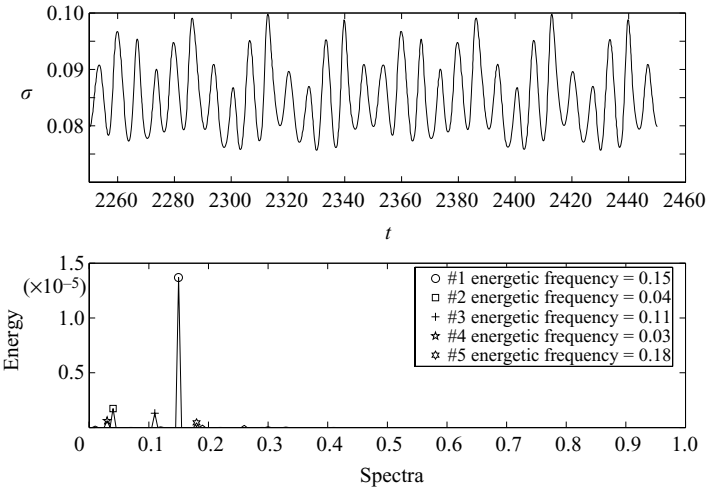

FIGURE 13. Spectra of the standard deviation of E at $Re = 525$ for case (II). $\Omega_{F_i} = 0.11, 0.15, 0.18$.

(a_1, a_2, a_3)	(1, 1, 1)	(1, 0, 0)	(0, 1, 0)	(0, 0, 1)	(3, 0, 0)	(0, 3, 0)	(0, 0, 3)
$\bar{E}$	1.1793	1.0474	1.1488	1.0089	1.1998	1.4029	1.0683
σ_E	0.0834	0.0389	0.1142	0.0088	0.1290	0.2054	0.0556

TABLE 4. Effect of different frequencies on E at $Re = 525$. Case I: $\Omega_{F,i} = 0.1, 0.15, 0.2$.

(a_1, a_2, a_3)	(1, 1, 1)	(1, 0, 0)	(0, 1, 0)	(0, 0, 1)	(3, 0, 0)	(0, 3, 0)	(0, 0, 3)
$\bar{E}$	1.1883	1.0523	1.1488	1.0142	1.2123	1.4029	1.1025
σ_E	0.0820	0.0423	0.1142	0.0133	0.1363	0.2054	0.0821

TABLE 5. Effect of different frequencies on E at $Re = 525$. Case II: $\Omega_{F,i} = 0.11, 0.15, 0.18$.

In many cases, the periodicity exhibits its effect only as a periodic variation at harmonics of a particular frequency. We next consider the first four harmonics in the K-L expansion (4.13) using $T = 1/0.15$. Without loss of generality, we consider the following random input:

$$\text{(III)}: Q(t) = \frac{4}{3}\left(1 + 0.1\sin 2\pi\Omega_F t + \eta\sqrt{\frac{2}{T}}\sum_{i=1}^{4}\sqrt{\lambda_i}\xi_i \sin(2\pi i\Omega_F t)\right), \tag{4.15}$$

with $\Omega_F = 0.15$, where $\xi_i \sim U[-1, 1]$ are uniform i.i.d. random variables with zero mean. We consider the following eigenvalues obtained from the periodic covariance kernel:

$$\lambda_i = 1.2266, 0.6504, 0.3080 \text{ and } 0.1493.$$

We take $\eta = 0.1/\sqrt{2\lambda_1/T}$ and the flow rate (4.15) can be rewritten as

$$Q(t) = \tfrac{4}{3}(1 + 0.2\xi \sin 2\pi\Omega_F t + S(t, \omega)),$$

where ξ is a uniform random variable in [0, 1] as before, and $S(t, \omega)$ can be regarded as the perturbation from the superharmonics. We use ME-gPC with $N = 8\times4\times2\times1 = 64$

$\bar{E}(Q_1)$	$\bar{E}(Q_2)$	$\sigma_E(Q_1)$	$\sigma_E(Q_2)$	$\bar{E}(Q_1)/\bar{E}(Q_2)$	$\sigma_E(Q_1)/\sigma_E(Q_2)$
1.4261	1.4029	0.1675	0.2054	1.0165	0.8155

TABLE 6. Effect of superharmonic frequencies on E at $Re = 525$ for case (III).

and $p = 2$ to achieve numerical convergence. Let Q_1 indicate the above flow rate and Q_2 the flow rate without $S(t, \omega)$. In table 6, we present the mean and standard deviation of E for Q_1 and Q_2. We observe that the superharmonic frequencies increase $\bar{E}$ by about 1.7% while decreasing σ_E about 18.5%, which is consistent with the observations from cases (I) and (II).

In summary, for a given geometry and random (periodically correlated) flow rate condition, there exists a critical frequency which is most effective for heat transfer enhancement. Furthermore, to reach the maximum heat transfer enhancement, such a critical frequency should be related to the largest eigenvalue, i.e. the largest degree of perturbation. Other frequencies are, in general, not effective for increasing $\bar{E}$; however, they can significantly decrease σ_E.

4.5. *Correlation between cross-flow velocity and temperature*

In Ghaddar *et al.* (1986*c*) the relation between cross-flow velocity and heat transfer enhancement was studied by deterministic simulations. The approach was to compare the optimal frequencies for cross-flow velocity and E. It was found that the two optimal frequencies agree with each other qualitatively although there exists a slight difference. We know that the cross-flow velocity is mainly due to the oscillation imposed in the inflow boundary condition (see Ghaddar *et al.* 1986*b*). Here we measure the relation between cross-flow velocity and temperature quantitatively using the correlation at reference points, which in turn reflects the influence of the imposed oscillating flow rate condition on the heat transfer enhancement.

Along the straight line $x = 3.20, -1.89 \leqslant y \leqslant 0.73$, we select 40 equidistant grid points, denoted as $y_i, i = 1, 2, \ldots, 40$. Specifically, we define the following five reference points (see figure 3): $A(3.20, -0.90)$, $B(3.20, -1.89)$, $C(3.20, -1.22)$, $D(3.20, -0.80)$ and $E(3.20, 0.71)$. We use v_i to denote the cross-flow velocity at grid y_i, and T_j the temperature at grid y_j. Let ρ denote the correlation between v_i and T_j. For each pair (v_i, T_j), we have the correlation

$$\rho_{ij} = \frac{\langle (v_i - \bar{v}_i)(T_j - \bar{T}_j) \rangle}{\sigma_{v,i}\sigma_{T,j}}, \tag{4.16}$$

where $\sigma_{f,i}$ denotes the standard deviation of the variable f. We know that $-1 \leqslant \rho_{ij} \leqslant 1$ and a large absolute value of ρ_{ij} corresponds to a large correlation. In figure 14, we plot the correlation matrix ρ_{ij} for uniform inputs with $\Omega_F = 0.15$ at $t = \hat{T}$, where $\hat{T}$ is the period of converged solutions. We can see that $|\rho_{ij}| \approx 1$ except in a narrow region, which implies that the cross-flow velocity and temperature are perfectly correlated. For any fixed v_i, $\rho_{ij} \approx -1$ for T_j at grid points $y_j \in [-1.89, -0.90]$, corresponding to the groove part; $\rho_{ij} \approx 1$ for T_j at grid points $y_j \in [-0.62, 0.73]$, corresponding to the channel part; ρ_{ij} increases quickly from -1 to 1 for T_j within the narrow interval $y_j \in [-0.90, -0.62]$. These observations are consistent with the flow physics. It is known that the cold fluid in the channel part would be forced into the downstream side of the cavity by the Tollmien–Sclichting travelling wave, then push the hot fluid from the upstream part of the groove into the channel part. Hence, if the cross-flow

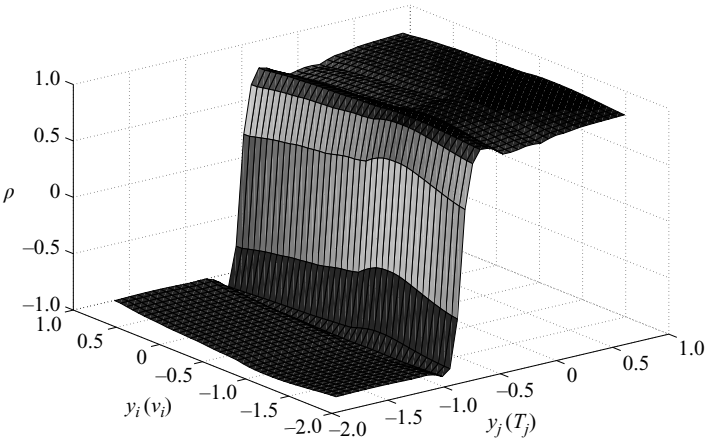

FIGURE 14. Correlation matrix ρ_{ij} for velocity–temperature pairs (v_i, T_j) on equidistant grid points along the straight line $x = 3.20, -1.89 \leqslant y \leqslant 0.73$. Uniform random inputs are used. $\Omega_F = 0.15$ and $Re = 525$.

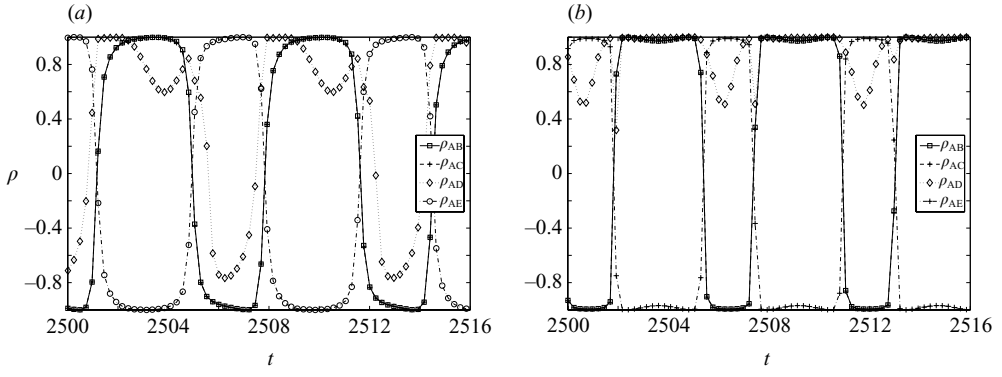

FIGURE 15. Evolution of ρ_{ij}. $\xi \sim U[0, 1]$ and $Re = 525$. (*a*) $\Omega_F = 0.15$; (*b*) $\Omega_F = 0.18$.

velocity v_i at a certain point y_i tends to increase, the temperature in the groove tends to decrease, corresponding to $\rho_{ij} \approx -1$, since the heat is from the groove to the channel; the temperature in the channel tends to increase, corresponding to $\rho_{ij} \approx 1$. Thus, the correlation ρ_{ij} indicates that the relation between the trends of v_i and T_j is almost linear, which implies that the evolution of temperature can be perfectly reflected by the evolution of cross-flow velocity.

In figure 15 we plot the time evolution of correlation between point A and other defined points (B, C, D and E) for $\Omega = 0.15$ in (*a*) and for $\Omega_F = 0.18$ in (*b*). We see that the correlation value switches between -1 and 1 periodically except for the points (ρ_{AD}) in the aforementioned narrow transient interval. The correlation for $\Omega_F = 0.18$ shows a sharper transition between -1 and 1, which implies that the cross-flow velocity and temperature are more correlated for $\Omega_F = 0.18$. This does not conflict with the fact that the optimal frequency is $\Omega_F = 0.15$. Since the optimal frequency corresponds to a larger response in the cross-flow velocity, which implies that the induced uncertainty is also larger, it is reasonable that the transition region of ρ_{ij} is larger for the optimal frequency. Since similar observations are obtained for other random inputs, the results are not presented here.

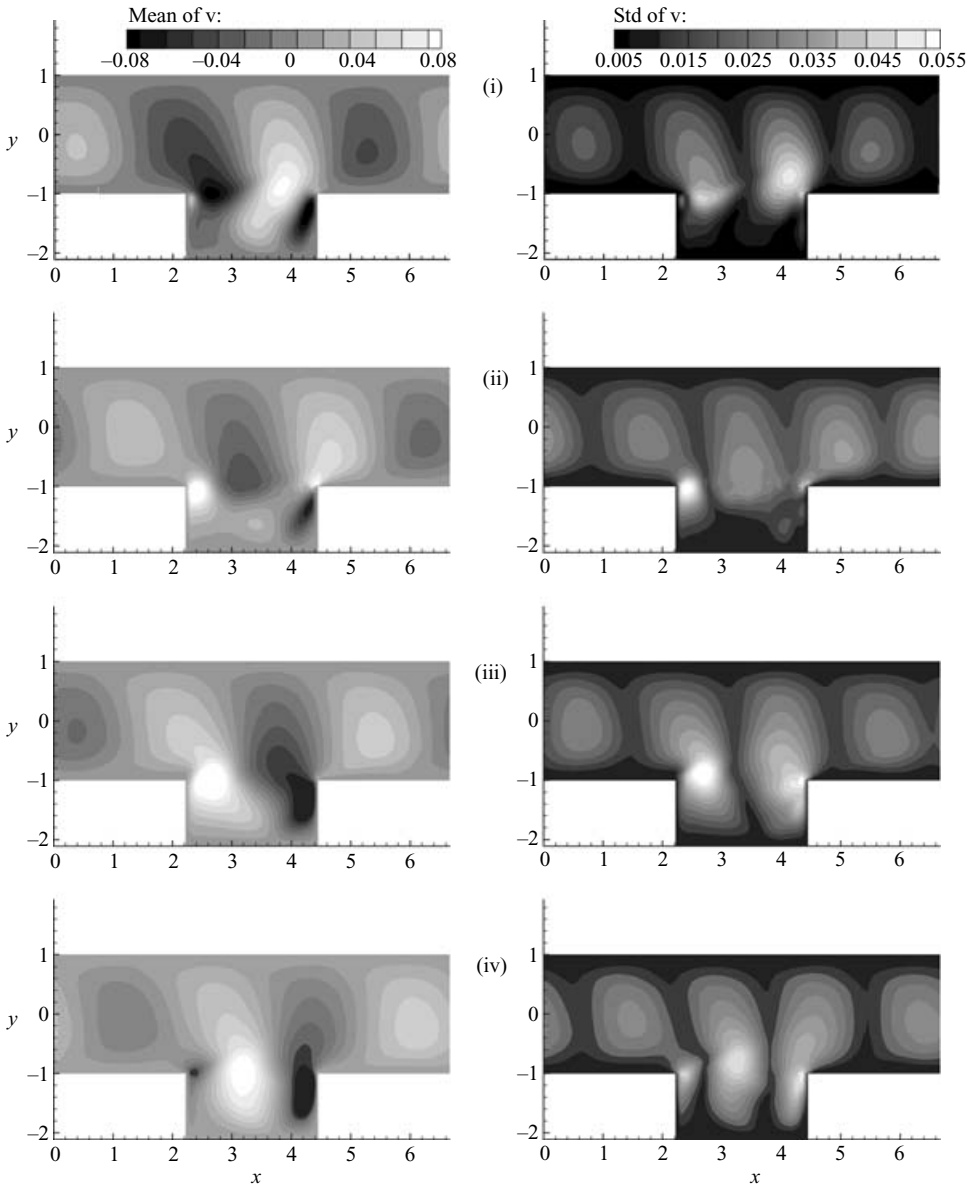

FIGURE 16. Mean (a) and standard deviation (b) of cross-flow velocity at (i) $t = \hat{T}/4$, (ii) $\hat{T}/2$, (iii) $3\hat{T}/4$, (iv) $\hat{T}$ with $\hat{T}$ being the period. $\xi \sim U[0, 1]$, $\Omega_F = 0.15$ and $Re = 525$.

4.6. *Visualizations*

In this section we present the visualization of the statistics of velocity and temperature. In figures 16 and 17, we show the mean (a) and standard deviation (b) of velocity and temperature fields, respectively, for $Re = 525$ within one period. Since there exists qualitative similarity between the corresponding statistics for the different random inputs, we present here only results for the uniform random inputs.

In figure 16, significant mixing at the groove lip is observed in the mean of cross-flow velocity. The largest standard deviation is located near the groove lip and

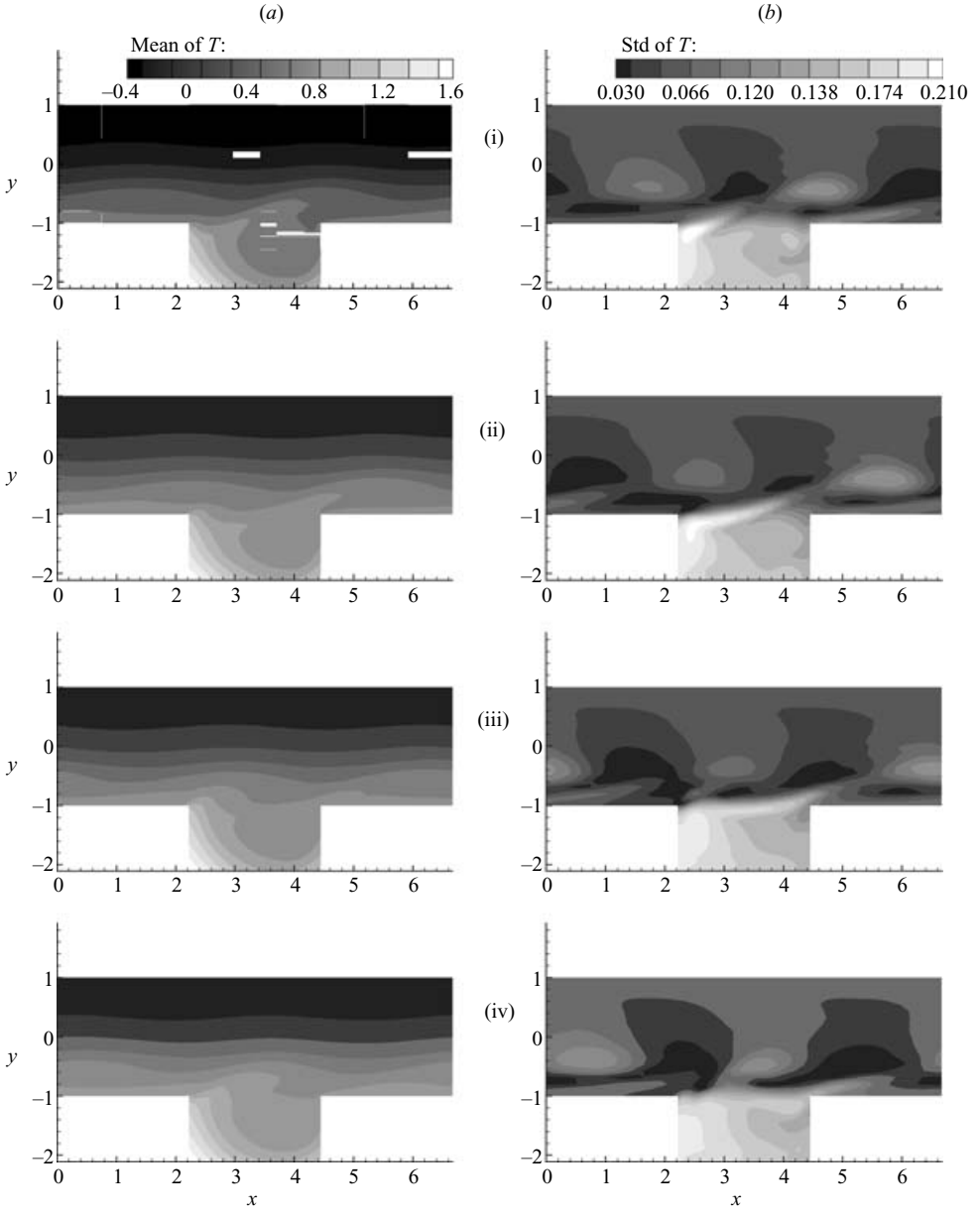

FIGURE 17. Mean (a) and standard deviation (b) of temperature at (i) $t = \hat{T}/4$, (ii) $\hat{T}/2$, (iii) $3\hat{T}/4$, (iv) $\hat{T}$ with $\hat{T}$ being the period. $\xi \sim U[0, 1]$, $\Omega_F = 0.15$ and $Re = 525$.

decreases into the channel and groove, which implies that the communication between the channel and groove is very sensitive to the excitation. In figure 17, a two-wave structure is observed in isocontours of the mean temperature field. Compared to corresponding deterministic results (see figure 3 in Ghaddar *et al.* (1986*c*)), the two-wave structure is not as pronounced because the amplitude 0.2 was used in Ghaddar *et al.* (1986*c*) while in our simulations the mean amplitude is 0.1 for a uniform random amplitude in [0, 0.2]. The largest standard deviation is inside the groove and along the groove lip; however, the standard deviation is small in the channel. By noting the

large cross-flow velocity along the groove lip and the property of correlation matrix ρ_{ij} discussed in the previous section, we know that it is the convection process that introduces large uncertainty to the temperature in the groove.

5. Summary

We have introduced a new modelling approach to studying unsteady convective heat transfer, where external excitations are introduced as stochastic processes rather than as prescribed deterministic functions. This approach is at least two to three orders of magnitude more efficient than performing standard Monte-Carlo simulations. There is currently growing interest in quantifying uncertainties in heat transfer, and new interesting methods are emerging (see Ghanem 1999*a*; Emery 2001; Wang & Zabaras 2005). These methods can also be employed to more effectively probe the sensitivities of the system and to gain insight into the flow physics and thermal processes, as we demonstrate here.

Specifically, we employed multi-element generalized polynomial chaos (ME-gPC) to investigate heat transfer enhancement in a two-dimensional grooved channel caused by a periodic flow oscillation of random amplitude; this geometry was first introduced in Ghaddar *et al.* (1986*c*). The stochastic mean results are in good agreement with the deterministic studies of Ghaddar *et al.* (1986*c*). In particular, we demonstrated that the deterministic results are embedded in the stochastic simulation results (see figure 9). This, in turn, implies that the ME-gPC technique is an effective approach not only for stochastic studies but also for obtaining deterministic results efficiently.

We first presented the mean values of the heat transfer enhancement parameter E along with lower and upper bounds, for different excitation frequencies and two different random inputs corresponding to uniform and Beta probability density functions (PDFs). At small excitation amplitudes, we found that the optimal frequency for heat transfer enhancement is $\Omega_F \approx 0.15$, which is close to the eigen-frequency of the least-stable mode $\Omega_1 = 0.142$ of Tollmien–Schlichting (T-S) channel waves at the same Reynolds number. We also demonstrated that the optimal frequency is a function of the amplitude of the excitation. For the optimal frequency $\Omega_F = 0.15$, we presented the PDFs of E, which were very different from the uniform and Beta PDFs of the stochastic inputs. In particular, we found that these PDFs are skewed towards larger values of E and their peaks increase and move to even larger values of E as the Reynolds number increases. This result can be exploited in future studies to design even more effective heat transfer enhancement strategies. More interestingly perhaps, the stochastic modelling approach offers the possibility of designing 'smart' PDFs of the stochastic input that can result in improved heat transfer enhancement rates.

We also studied the relation between E and the amplitude of the imposed perturbation based on the PDFs of E for uniform random inputs. For a low Reynolds number, e.g. $Re = 225$, a linear relation between E and the amplitude is observed for large E; however, such a relation becomes strongly nonlinear as the Reynolds number increases. We also studied the effect of frequencies on E using random excitations with different frequencies (one is the optimal frequency $\Omega_F = 0.15$, the other frequencies are relatively far way from the optimal one.) Compared to the optimal frequency $\Omega_F = 0.15$, it appears that other frequencies can reduce the standard deviation effectively but they affect the mean value very little. Finally, we demonstrated the strong connection between the cross-flow velocity and temperature through the correlation matrix. This analysis provided good evidence of the contribution of T-S travelling waves to effective heat transfer enhancement.

This work was supported by the NSF-Sandia program and partially by AFOSR. The computations were performed at NSF supercomputing centers (SDSC, NCSA and PSC). Preliminary results were presented at the ASME Summer Heat Transfer Conference (July 2005, San Francisco) in a symposium in honor of Professor B. B. Mikic of MIT, who first suggested this heat transfer enhancement problem.

Appendix A. Application of ME-gPC to Navier–Stokes equations

In § 2, it is shown that the support of the random variable $\boldsymbol{\xi}$ can be decomposed into N random elements e_k, $k = 1, 2, \ldots, N$. In each element e_k a new random variable $\boldsymbol{\xi}_k$ with a PDF $f_k(\boldsymbol{\xi}_k)$ is defined. We note that $\boldsymbol{\xi}_k$ is defined in $[-1, 1]^d$. Using $f_k(\boldsymbol{\xi}_k)$ as a weight function, we can construct a set of orthogonal polynomials $\{\Phi_{k,i}(\boldsymbol{\xi}_k)\}$ satisfying

$$\mathbb{E}_k[\Phi_{k,i}\Phi_{k,j}] = \mathbb{E}_k[\Phi_{k,i}^2], \tag{A 1}$$

where $\mathbb{E}_k[\cdot]$ indicates expectation with respect to PDF $f_k(\boldsymbol{\xi}_k)$.

To employ ME-gPC we need to expand all the random fields spectrally in each random element e_k. Given the local polynomial chaos basis $\{\Phi_{k,i}(\boldsymbol{\xi}_k)\}$, the random fields, e.g. $\boldsymbol{v}$, Π and θ, can be expressed in random elements e_k as

$$\boldsymbol{v} = \sum_{i=0}^{N_p} \boldsymbol{v}_{k,i}\Phi_{k,i}, \quad \Pi = \sum_{i=0}^{N_p} \Pi_{k,i}\Phi_{k,i}, \quad \theta = \sum_{i=0}^{N_p} \theta_{k,i}\Phi_{k,i}, \tag{A 2}$$

where p is the polynomial order and N_p is the total number of modes given by $(d + p)!/d!p!$. Substituting (A 2) into equations (3.4) and (3.11) and performing a Galerkin projection in terms of each mode in $\{\Phi_{k,i}\}$, we obtain the following deterministic PDE system:

$$\frac{\partial \boldsymbol{v}_{k,m}}{\partial t} + \boldsymbol{N}_{k,m} = -\hat{\Pi}_{k,m} + Re^{-1}\nabla^2\boldsymbol{v}_{k,m} + \Pi_{k,m}^{x}\hat{\boldsymbol{x}}, \quad \nabla\cdot\boldsymbol{v}_{k,m} = 0, \tag{A 3a, b}$$

$$\frac{\partial \theta_{k,m}}{\partial t} + \frac{1}{\mathbb{E}_k[\Phi_{k,m}^2]}\sum_{i=0}^{N_p}\sum_{j=0}^{N_p} c_{ijm}^k \nabla\cdot\boldsymbol{H}_{i,j} = (RePr)^{-1}\nabla^2\theta_{k,m}, \tag{A 3c}$$

where $c_{ijm}^k = \mathbb{E}_k[\Phi_{k,i}\Phi_{k,j}\Phi_{k,m}]$, $\hat{\boldsymbol{x}}$ denotes the unit vector in the x-direction, $\boldsymbol{H}_{i,j} = \boldsymbol{v}_{k,i}(\theta_{k,j} + \gamma_{k,j}x)$ and

$$\boldsymbol{N}_{k,m} = \frac{1}{\mathbb{E}_k\left[\Phi_{k,m}^2\right]}\sum_{i=0}^{N_p}\sum_{j=0}^{N_p} c_{ijm}^k[(\boldsymbol{v}_{k,i}\cdot\nabla)\boldsymbol{v}_{k,j}], \tag{A 4}$$

$m = 0, 1, \ldots, N_p$. The same procedure can be applied for the boundary conditions to complete the above PDE system.

To this end we obtain a complete deterministic PDE system in each random element e_k. The structures of these PDE systems are the same except for some constant parameters, e.g. c_{ijm}^k. Thus, a unique procedure can be developed for the temporal discretization of equations (A 3), which can be found in Wan (2006).

Appendix B. The postprocessing stage

We integrate equations (A 3) and obtain the local polynomial expansions (A 2). We subsequently use the temperature field $T(\boldsymbol{x}, t; \omega)$ as an example to present the formulae for the commonly used statistics: mean $M(T)$, variance $V(T)$, skewness $S(T)$ and kurtosis $K(T)$.

For any fixed $\boldsymbol{x}$ and t, we know the local mean is $T_{k,0}$ due to the orthogonality of the local polynomial basis $\{\Phi_{k,i}\}$. Using the formula (2.5), we obtain the global mean:

$$M(T) \approx \sum_{k=1}^{N} Pr(\boldsymbol{\xi} \in e_k) T_{k,0}. \tag{B 1}$$

The global variance can be expressed as

$$V(T) = \mathbb{E}[T^2] - M^2(T) \approx \sum_{k=1}^{N} Pr(\boldsymbol{\xi} \in e_k) \sum_{i=0}^{N_p} T_{k,i}^2 \mathbb{E}_k\left[\Phi_{k,i}^2\right] - M^2(T). \tag{B 2}$$

Using the global mean and variance, we can obtain the global skewness and kurtosis, respectively,

$$\begin{aligned} S(T) &= V^{-3/2}(T)\mathbb{E}[(T - M(T))^3] \\ &= V^{-3/2}(T)[\mathbb{E}[T^3] - 3M(T)V(T) - M^3(T)] \\ &= V^{-3/2}(T) \sum_{k=1}^{N} Pr(\boldsymbol{\xi} \in e_k) \sum_{i=0}^{N_p} \sum_{j=0}^{N_p} \sum_{m=0}^{N_p} T_{k,i} T_{k,j} T_{k,m} \mathbb{E}_k[\Phi_{k,i} \Phi_{k,j} \Phi_{k,m}] \\ &\quad - V^{-3/2}(T)(3M(T)V(T) + M^3(T)), \end{aligned} \tag{B 3}$$

$$\begin{aligned} K(T) &= V^{-2}(T)\mathbb{E}[(T - M(T))^4] \\ &= V^{-2}(T)[\mathbb{E}[T^4] - 4M(T)\mathbb{E}[T^3] + 6M^2(T)V(T) + 3M^4(T)] \\ &= V^{-2}(T) \sum_{k=1}^{N} Pr(\boldsymbol{\xi} \in e_k) \sum_{i=0}^{N_p} \sum_{j=0}^{N_p} \sum_{m=0}^{N_p} \sum_{n=0}^{N_p} T_{k,i} T_{k,j} T_{k,m} T_{k,n} \mathbb{E}_k[\Phi_{k,i} \Phi_{k,j} \Phi_{k,m} \Phi_{k,n}] \\ &\quad - 4V^{-2}(T)M(T) \sum_{i=0}^{N_p} \sum_{j=0}^{N_p} \sum_{m=0}^{N_p} T_{k,i} T_{k,j} T_{k,m} \mathbb{E}_k[\Phi_{k,i} \Phi_{k,j} \Phi_{k,m}] \\ &\quad + V^{-2}(T)[6M^2(T)V(T) + 3M^4(T)]. \end{aligned} \tag{B 4}$$

REFERENCES

Amon, C. H., Majumdar, D., Herman, C. V., Mayinger, F. & Mikic, B. B. 1992 Numerical and experimental studies of self-sustained oscillatory flows in communicationg channels. *Intl J. Heat Mass Transfer* **35**, 3115–3129.

Amon, C. H. & Mikic, B. B. 1985 Numerical prediction of convective heat transfer in self-sustained oscillatory flows. *J. Thermophys. Heat Transfer* **4** (2), 239–246.

Babuška, I., Tempone, R. & Zouraris, G. E. 2004 Galerkin finite element approximations of stochastic elliptic differential equations. *SIAM J. Numer. Anal.* **42** (2), 800–825.

Canavan, G. H. 1970 Some properties of a Lagrangian Wiener-Hermite expansion. *J. Fluid Mech.* **41**, 405–412.

Chorin, A. J. 1974 Gaussian fields and random flow. *J. Fluid Mech.* **63**, 21–32.

Chung, Y. M. & Tucker, P. G. 2004 Numerical studies of heat transfer enhancements in laminar separated flows. *Intl J. Heat Fluid Flow* **25**, 22–31.

Crow, S. C. & Canavan, G. H. 1970 Relationship between a Wiener-Hermite expansion and an energy cascade. *J. Fluid Mech.* **41**, 387–403.

Deb, M. K., Babuška, I. & Oden, J. T. 2001 Solution of stochastic partial differential equations using Galerkin finite element techniques. *Comput. Methods Appl. Mech. Engng* **190**, 6359–6372.

Emery, A. 2001 Higher order perturbation analysis of stochastic thermal systems with correlated uncertain properties. *Trans. ASME J. Heat Transfer* **123** (2), 390–399.

Frauenfelder, P., Schwab, C. & Todor, R. A. 2005 Finite elements for elliptic problems with stochastic coefficients. *Comput. Methods Appl. Mech. Engng* **194**, 205–228.

Ghaddar, N. K., Karniadakis, G. E. & Patera, A. T. 1986*a* A conservative isoparametric spectral element method for forced convection; application to fully developed flow in periodic geometries. *Numer. Heat Transfer* **9**, 277–300.

Ghaddar, N. K., Magen, M., Mikic, B. B. & Patera, A. T. 1986*b* Numerical investigation of incompressible flow in grooved channels. Part 1. Stability and self-sustained oscillations. *J. Fluid Mech.* **163**, 99–127.

Ghaddar, N. K., Magen, M., Mikic, B. B. & Patera, A. T. 1986*c* Numerical investigation of incompressible flow in grooved channels. Part 2. Resonance and oscillatory heat transfer enhancement. *J. Fluid Mech.* **168**, 541–567.

Ghanem, R. G. 1999*a* Higher order sensitivity of heat conduction problems to random data using the spectral stochastic finite element method. *Trans. ASME J. Heat Transfer* **121**, 290–299.

Ghanem, R. G. 1999*b* Ingredients for a general purpose stochastic finite element formulation. *Comput. Methods Appl. Mech. Engng* **168**, 19–34.

Ghanem, R. G. 1999*c* Stochastic finite elements for heterogeneous media with multiple random non-gaussian properties. *ASCE J. Engng Mech.* **125** (1), 26–40.

Ghanem, R. G. & Spanos, P. 1991 *Stochastic Finite Elements: A Spectral Approach*. Springer.

Gladyshev, E. G. 1961 Periodically correlated random sequences. *Sov. Math.* **2**, 385–388.

Greiner, M. 1991 An experimental investigation of resonant heat transfer enhancement in grooved channels. *Intl J. Heat Mass Transfer* **34**, 1383–1391.

Herman, C. & Kang, E. 2001 Experimental visualization of temperature fields and study of heat transfer enhancement in oscillatory flow in a grooved channel. *J. Heat Mass Transfer* **37**, 87–99.

Hogge, H. D. & Meecham, W. C. 1978 The Wiener-Hermite expansion applied to decaying isotropic turbulence using a re-normalized time-dependent base. *J. Fluid Mech.* **85**, 325–347.

Holden, H., Oksendal, B., Uboe, J. & Zhang, T. 1996 *Stochastic Partial Differential Equations: A Modeling, White Noise Functional Approach*. Birkhauser.

Kahng, W.-H. & Siegel, A. 1970 The Cameron-Martin-Wiener method in turbulence and in burgers' model: general formulae and application to late decay. *J. Fluid Mech.* **41**, 593–618.

Kaminski, M. & Carey, G. F. 2005 Stochastic perturbation-based finite element approach to fluid flow problems. *Intl J. Numer. Meth. Heat Fluid Flow* **15** (7), 671–697.

Kaminski, M. & Hien, T. D. 1999 Stochastic finite element modeling of transient heat transfer in layered composites. *Intl J. Numer. Meth. Heat Fluid Flow* **26** (6), 791–800.

Karniadakis, G. E. & Sherwin, S. J. 2005 *Spectral/* hp *Element Methods for CFD*. Oxford University Press.

Lototsky, S., Mikulevicius, R. & Rozovskii, B. L. 1997 Nonlinear filtering revisited: a spectral approach. *SIAM J. Control Optim.* **35** (2), 435–461.

Lucor, D. 2004 Generalized polynomial chaos: applications to random oscillators and flow-structure interactions. PhD thesis, Brown University, Division of Applied Mathematics.

Mikulevicius, R. & Rozovskii, B. L. 2004 Stochastic navier-stokes equations for turbulent flow. *SIAM J. Math. Anal.* **35** (5), 1250–1310.

Orszag, S. A. & Bissonnette, L. R. 1967 Dynamical properties of truncated Wiener-Hermite expansions. *Phys. Fluids* **10** (12), 2603–2613.

Patera, A. T. & Mikic, B. B. 1986 Exploiting hydrodynamic instabilities. resonant heat transfer enhancement. *Intl J Heat Mass Transfer* **29**, 1127–1138.

Wan, X. 2006 Multi-element generalized polynomial chaos for differential equations with random imputs: algorithms and applications. PhD thesis, Brown University, Division of Applied Mathematics.

Wan, X. & Karniadakis, G. E. 2005 An adaptive multi-element generalized polynomial chaos method for stochastic differential equations. *J. Comput. Phys.* **209** (2), 617–642.

Wan, X. & Karniadakis, G. E. 2006 Multi-element generalized polynomial chaos for arbitrary probability measures. *SIAM J. Sci. Comput.* **28** (3), 901–928.

Wang, J. & Zabaras, N. 2005 Using Bayesian statistics in the estimation of heat source in radiation. *Intl J. Heat Mass Transfer* **48**, 15–29.

Wiener, N. 1938 The homogeneous chaos. *Am. J. Math.* **60**, 897–936.

Xiu, D. & Karniadakis, G. E. 2002 The Wiener-Askey polynomial chaos for stochastic differential equations. *SIAM J. Sci. Comput.* **24** (2), 619–644.

Xiu, D. & Karniadakis, G. E. 2003 Modeling uncertainty in flow simulations via generalized polynomial chaos. *J. Comput. Phys.* **187**, 137–167.